A Planar Integrated Folded Reflectarray Antenna with Circular Polarization

Chong Zhang, Yongfeng Wang, Fuguo Zhu, Gao Wei, Jianzhou Li and Steven Gao

Abstract—Folded reflectarray is very important for satellite communications due to advantages of low profile and high gain. Traditionally, a fold reflectarray employs a horn as a feed source in the centre of antenna structure, making it complicated in fabrication and difficult to integrate the antenna into a planar structure. In addition, it can achieve linear polarization only. This paper presents the complete design of the 1st folded reflectarray with circular polarization. To achieve circular polarization (CP), a printed meander-line polarizer is designed and integrated with the folded reflectarray. To reduce the fabrication complexity and achieve a low-profile planar structure, a small 2×2 planar array is designed as the feed source instead of a horn. Thus the whole antenna, including the feed source, folded reflectarray and meander-line polarizer can be fully integrated and fabricated using low-cost PCB technology. To validate the concept, a CP folded reflectarray is designed, fabricated and measured. Details of designs of feed source, folded reflectarray, and meander-line polarizer are presented and discussed. The antenna reflection coefficient is less than -10 dB and the axial ratio covering the 3 dB main-lobe angle range is less than 3 dB over a bandwidth from 5.1 to 5.5 GHz. In addition, the maximum boresight gain of 22 dBi is obtained. The antenna has high gain, low profile, planar structure, low cost and is fully integrated, thus promising for applications in satellite communications.

Index Terms—linear polarization, circular polarization, meander-line polarizer, folded reflectarray

I. INTRODUCTION

DUE to the combination of the advantages from the printed microstrip array antenna and reflector antenna, the reflectarray antenna [1] has demonstrated its potential as an important and popular high-gain antenna for the point-to-point communication systems. As one distinctive member among the reflectarray family, the folded reflectarray (FRA) [2] successfully reduces the antenna volume by employing the dual-polarized unit-cells for polarization conversion and placing a polarizer grid right above it, as shown in Fig.1.

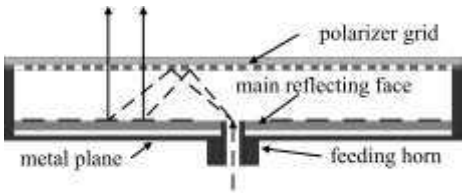

Fig. 1. General configuration of the LP FRA structure [2]

During recent years, many folded reflectarray antennas with different functions for various applications have been reported. In [3] and [4], the folded reflectarray with shaped beam pattern is used for foreign object debris detection on runways and the local multipoint distribution services. And in [5], a Q-band folded reflectarray using the planar SIW as the primary source is designed for the high data rate communications. For the dual-frequency application, a folded reflectarray operating at both 20 GHz and 30 GHz is accomplished in [6]. In addition, a millimeter-wave folded reflectarray with the mechanical beam scanning capability is presented in [7]. The folded reflectarray is also introduced to the space communication area. For example, the Ka-band smart folded reflectarray antenna for the SatCom-on-the-move system [8][9] has been reported and the electrical beam scanning capability has been achieved successfully. Compared with the reflector antenna, the utilization of the FRA reduces the height of antenna for the user terminals, which is very useful for mobile communications. Moreover, compared with the traditional microstrip array antenna, the power loss in FRA at mm-wave band is significantly reduced due to the use of spatial power combining instead of microstrip feed networks.

There are two main problems of FRA, however. One problem is that it can only produce linear polarization; the second problem is that it usually employs a horn as the feed source at the center of the antenna structure. The horn has a 3D structure and is not compatible with reflectarray structure made of PCB, thus the whole antenna structure is complicated for fabrication and assembly and the cost is high. For mobile satellite communications, ideally it requires an antenna which has a fully integrated planar structure, low profile, CP and high gain, and can be easily fabricated using the low-cost PCB technology, The aim of our work is to fill this gap.

Due to the use of the polarization selective grid, however, one problem of the FRA is that it can only produce linear polarizations (LP) while some application areas require circularly polarized antennas, especially the satellite communications due to Farady effects in the ionosphere [10]. Then, it becomes a necessary choice to figure out an easy way to expend the FRA polarization fashion. Therefore, employing

Chong Zhang, Yongfeng Wang, Gao Wei and Jianzhou Li are with School of Electronics and Information, Northwestern Polytechnical University, Xi'an, Shaanxi, 710129 P.R.China. (Email: zczcdale@163.com).

Fuguo Zhu, is with Science and Technology on Antenna and Microwave Laboratory, Nanjing Research Institute of Electronics, Nanjing, 210039, China. (Email: zhu.fuguo@hotmail.com)

Steven Gao is with School of Engineering and Digital Arts, University of Kent, Canterbury, CT2 7NT, UK (Email: S.Gao@kent.ac.uk).

a polarizer to realize the linear-to-circular polarization conversion based on the original linear-polarized FRA has been considered.

The meander-line polarizer, as the most widely used type, has been carried out to realize the linear-to-circular polarization conversion since 40 years ago [11], in particular the multi-layer one [12][13] which provides the wider bandwidth and lower reflection than the single layer one.

Therefore, through putting a classic three-layer meander-line polarizer on the top of the fundamental linear-polarized FRA, a circularly polarized FRA in C-band is obtained in this paper. In Section Ⅱ, the component function and the basic operating principle of the CP FRA is clarified respectively. In Section Ⅲ, the configuration of dual-linear-polarized unit-cell, the single-linear-polarized element of the integrated feeding array, and the unit meander-line are depicted in detail. Then, the performance of the proposed unit-cells is characterized by the simulated results. Otherwise, the realizable phase compensation range of the dual-linear-polarized unit-cell is investigated. In Section Ⅳ, the central integrated feeding array and the corresponding four-way T-junction feeding network is introduced. On the basis of the previous preparation, the LP FRA is prototyped and its performance is characterized through measured results. In the end of this section, the final CP FRA is built up and tested. In addition, the discussions about the measured results are presented. At last, the conclusion is drawn and presented in Section Ⅴ.

II. CP FRA OPERATING PRINCIPLE

In Fig. 2, the general configuration of the CP FRA structure and the wave propagation path are shown. The CP FRA is consisted of four main components, including the reflecting face for polarization twisting and phase compensation, the polarization selecting grid , the central feeding source (horn or array) and the three-layer meander-line polarizer for linear-to-circular polarization conversion. As illustrated in Fig. 2, the wave is transmitted from the feeding source to the polarizer grid. Because of the parallel polarization with the grid vein, the wave (marked with dash line) is mirror reflected and illuminate backwards to the reflecting face. Here, one hypothesis is previously set that the incident wave within the aperture of the reflecting face is received perfectly.

The dual-linear-polarized unit cells are used in the reflecting face. After twisting the polarization and compensating the path difference (using true-time delay-line or other phase compensation methods), the incident wave is reradiated towards the polarizer grid and penetrates it still with the linear polarization but in the perpendicular direction (marked with solid line).

Besides the common components in the fundamental LP FRA, a classic three-layer meander-line polarizer is placing on the top of the whole antenna structure with a 45 degree twisting along the grid vein. Finally, through utilizing the linear-to-circular polarizer, the CP wave (marked with dot line) is realized.

III. UNIT-CELL DESIGNS

According to the antenna principle description, the CP FRA design could be decomposed into the performance evaluation of each main component. From the perspective of the design procedure and simulations, every main component is consisted of periodically duplicated unit-cells. Thus, before building up the final CP FRA, the performance of these unit-cells in these four main components should be carefully investigated in the first place.

A. Configuration and performance of the unit-cells in the reflecting face

Due to the simple structure, low cost and ease of fabrication, the most widely used unit cell in the reflecting face is the reflection-type rectangular varied-size microstrip patch. However, the small idle-space in every unit-cell domain, which is mainly restricted by the single-layer stack-up structure, limits the application of the integrated chips (such as the phase shifter) in FRAs. For the future antenna function extension, the multi-layered transmission-type unit cell is used in the presented design.

In addition, the alternated feeding source is attempted to simplify the antenna mounting and lower the cost based on the existing design scheme. Thus, the widely used classic feeding horn is replaced by an integrated designed LP four-element feeding array. It is designed with the same stack-up structure and fabricated in the central position on the same board using PCB technology. Also, in order to provide a quansi-periodical

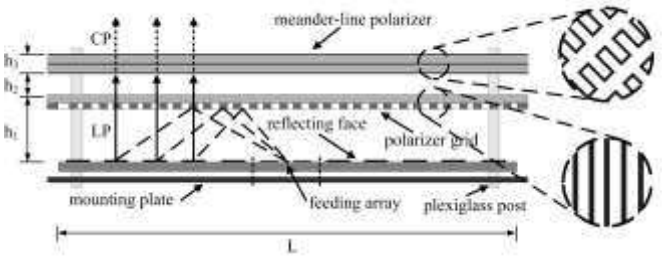

Fig. 2. General configuration of the CP FRA structure in side-view

condition for the neighboring unit-cells surrounding the feeding area, the configuration of the four feeding elements are inherited from the dual-linear-polarized unit-cells as much as possible.

The layouts and stack-up structures of the four-layer slot-type cavity-backed microstrip unit-cells with dual-and single-linear polarization are shown in Fig.3. The inner loop slot in the central, the outer loop slot surrounding the whole unit-cell structure and the metal vias comprise two back cavities resonating at adjacent frequency to broaden the operation bandwidth [13]. In the second layer of the stack-up, the strip feeding lines with the characteristic impedance of 63Ω for two perpendicular polarizations are placed under the inner loop slot for impedance matching and followed by the 50Ω ones. In the LP feeding element, the whole feeding structure are preserved while one metal vias nearby the outer loop slot is added and the short lines are connected between one feeding stripline and the ground both in the first and the fourth layer to eliminate the radiation in the corresponding polarization. In the fourth layer, the 50Ω microstrip feeding line is connected with the strip feeding line through the quasi-coaxial transition with the 50Ω impedance, which is consisted of four surrounding metal-through holes and one central signal metal-through hole. The structure dimensions of the element are partly listed in Table Ⅰ.

The four-layer stack-up structure is consisted of two two-layer PCB board (0.017mm copper thickness) and two substrate slabs. The employed material is PTFE fibreglass with the relative permittivity value of 2.65. The overlayer on

TABLE II
SUBSTRATE THICKNESS

	Substrate1	Substrate2	Substrate3	Substrate4
Thickness in mm	1.2~2.4	0.8	2	0.6

the top of Layer 1 name Substrate 1 in Fig.3 is used to decrease the unit-cell dimension and, as the additional function, to adjust the frequency shift casually caused by the manufacture error and the permittivity instability through modifying the substrate thickness. The applied substrate thickness is depicted in Table Ⅱ.

The simulated results over the operating bandwidth of the unit-cells in the main reflecting face are obtained under the

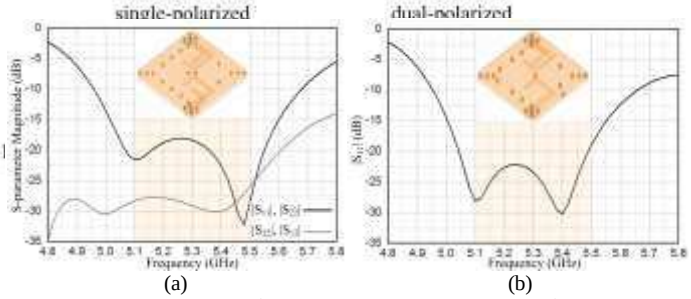

(a) (b)

Fig. 4. Simulated results of (a) the dual-polarized unit-cell for twisting and phase compensation and (b) the single-polarized unit-cell for feeding array

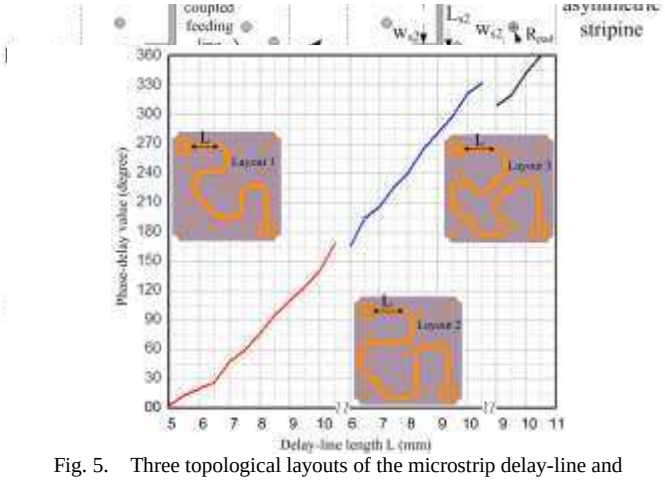

Fig. 5. Three topological layouts of the microstrip delay-line and phase-delay value

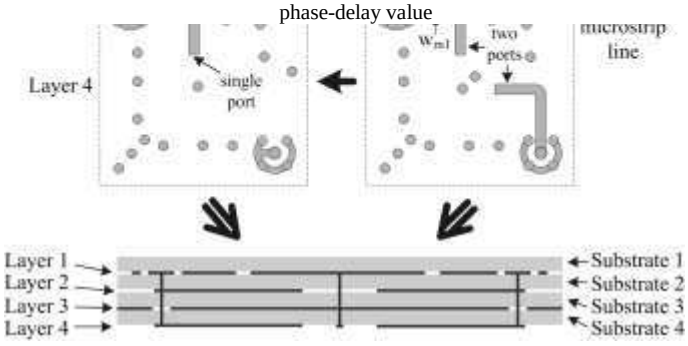

Fig. 3. Layouts of the single polarized element in the source array and the dual-polarized unit-cell for the FRA and the stack-up in side-view

periodical boundary condition and shown in Fig.4. Due to the symmetric structure distribution, the results of the two feeding ports in the dual-linear-polarized unit-cell are the same and overlapped in Fig.4 (a). And the coupling coefficient between the two ports is observed to be lower than -25dB. In Fig.4 (b), the $|S_{11}|$ result of single-polarized unit-cell for feeding array is shown.

According to the distribution of the soldering pads on the fourth layer, three topological layouts of the microstrip

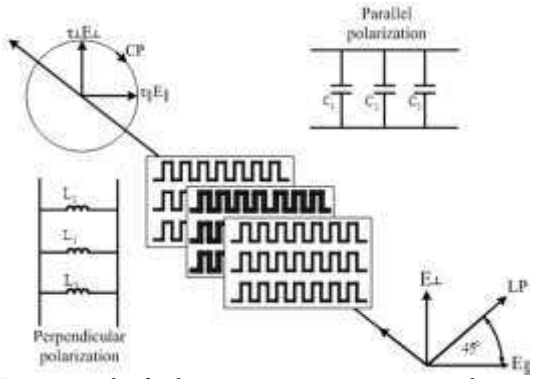

Fig. 6. Basic principle of polarization converting operation and circuit model for parallel polarization and perpendicular polarizations.

delay-line are prepared to cover a 360° phase delaying range, as shown in Fig.5. The transmission-type phase-delay manner is implemented through connecting the two feeding ports of the dual-linear-polarized unit-cell with the 50Ω microstrip line. Through changing the length of the microstrip delay-line, the 0°~170°, 165°~330° and 310°~360° phase delay range has been produced by Layout 1, Layout 2 and Layout 3 respectively. In order to decrease the return loss, the bent

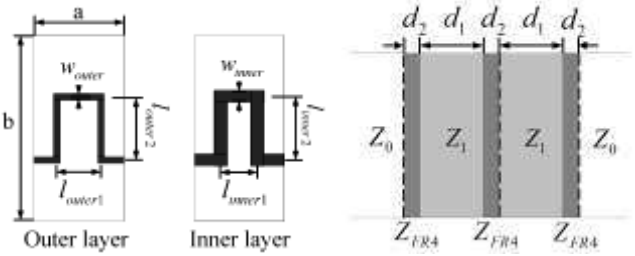

Fig. 7. General configuration of the three-layer meander-line polarizer and the stack-up in side-view

W_{c1} | W_{c2} | L_{c1} | L_{c2} | L_{c3}

TABLE III

DIMENSIONS OF THE UNIT-CELL IN THE MEANDER-LINE POLARIZER (MM)

a	b	w_{inner}	$l_{inner\,1}$	$l_{inner\,2}$
12.0	20.0	2.0	6.0	7.0
w_{outer}	$l_{outer\,1}$	$l_{outer\,2}$	d_1	d_2
0.6	6.0	7.8	12	0.6

corners is used in the delay-line layout.

B. Configuration and performance of the unit-cells in the meander-line polarizer

The basic principle of the meander-line polarizer with three sheets is briefly shown in Fig.6. The incident electric field is decomposed into two orthogonal polarizations, i.e., the perpendicular field and the parallel field ($E_\perp$ and $E_\parallel$). To obtain an ideal CP plane wave without losses, the

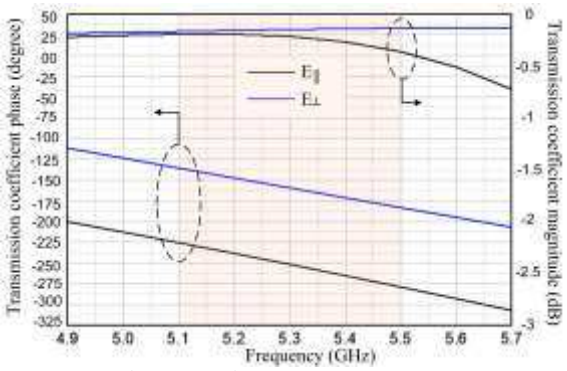

Fig. 8. General configuration of the three-layer meander-line polarizer and the stack-up in side-view

magnitudes of the transmission coefficient must be equal to unity for both orthogonal polarizations and the phase difference between them must be in quadrature [11].

The unit meander-line configuration and the stack-up sandwich are presented in this part, as shown Fig.7. The dimensions of the unit meander-line and the thickness of the each layer are listed in Table III. The meander-line is printed on the FR-4 Board with the relative permittivity value of 4.3 and the low foamed polyvinyl chloride with the relative permittivity value of 1.4 is used as the substrate slabs between the inner and outer meander-line layers.

The simulated transmission coefficient results of the unit meander-line over the operating bandwidth are shown in Fig.8. The phase difference between two perpendicular polarizations is 93°± 2°, and the magnitude difference is no more than 0.2 dB, which guarantee a proper circular-polarization performance for the following CP FRA design.

IV. CIRCULAR-POLARIZED FOLDED REFLECTARRAY

As indicated above, the performance of the unit cells has already been characterized by the simulated results. In this section, the performance of each main component in the proposed CP FRA will be validated through the measured results.

A. Integrated 2×2 feeding source array

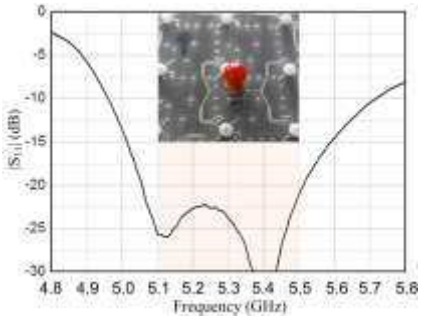

Fig.10. Measured $|S_{11}|$ result of the feeding array

On account of the single-polarized feeding unit-cell presented in the previous section, the space feeding array which is consisted of four elements in the centre of the main reflecting face and its mating four-way two-level T-junction power divider are illustrated in Fig.9. In order to minimize the divider size and lay the divider in the space between the pads prepared for the PCB manufacturing process, the impedance matching is realized at the same time as the power splitting and the first-level T structure is combined with the feeding SMA connector. The modified SMA connector (all pins with the length of 1.2mm) is standing soldered on the feeding point and the two bent bone-shape pads.

The measured reflection coefficient result of the proposed feeding array is shown in Fig. 10. The bandwidth with $|S_{11}|$ lower than -10 dB is from 4.95 GHz to 5.7GHz, which covers the operating frequency range and in this coverage, $|S_{11}|$ is lower than -20dB.

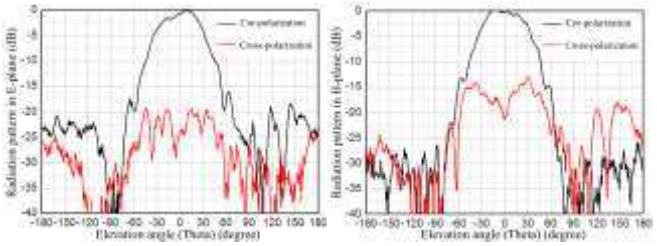

(a) 5.1 GHz

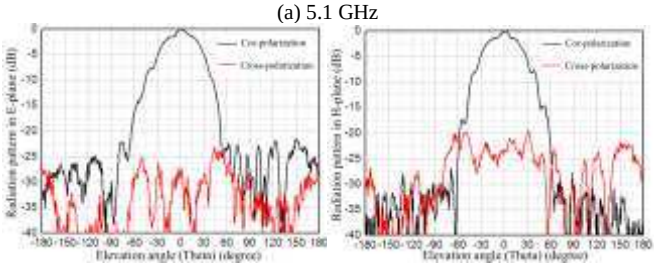

(b) 5.3 GHz

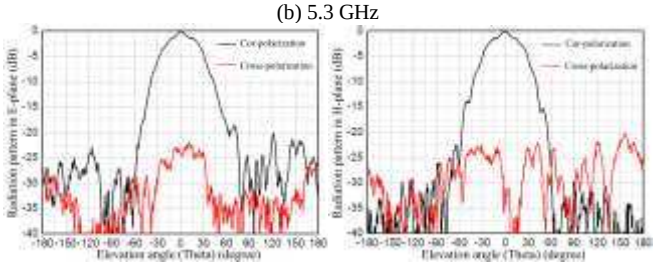

(c) 5.5 GHz

Fig.11. Measured normalized radiation pattern of the feeding array in E-plane and H-plane at (a) 5.1 GHz (b) 5.3 GHz and (c) 5.5 GHz

The measured normalized radiation patterns in both E-plane and H-plane at 5.1 GHz, 5.3 GHz and 5.5 GHz including the co-polarization and cross-polarization are shown in Fig. 11. The 10 dB dropping point of the normalized co-polarized pattern is aiming at around ±45° direction, which is approximately agreed with a $\cos^q$(theta) (q=5) curve. The normalized cross-polarization radiation level is mostly lower than -20 dB, while the level is higher than -15 dB in around ±30° direction of the H-plane radiation pattern at 5.1 GHz, as shown in Fig. 11(a). The cross-polarization radiation is mainly contributed by the re-radiation from the neighboring dual-polarized unit-cells (receiving the directly coupling from the feeding elements and transiting in the perpendicular polarization).

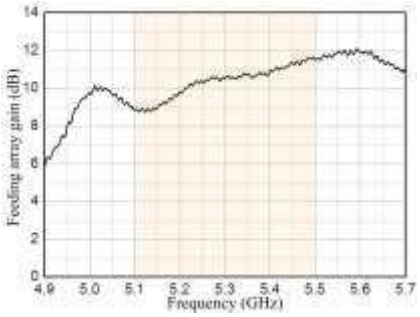

Fig.12. Antenna gain of the feeding array in broadside

Fig. 12 shows the measured antenna gain of the feeding array. There is a downwarping at around 5.15 GHz, which is caused by the radiation misalign shown in Fig. 11(a). Within the operating frequency bandwidth, the antenna gain climbs up to 11.6 dB at 5.5 GHz.

B. Configuration description of the propose FRA

The proposed CP FRA is built up on the base of a classic linear-polarized FRA through the employment of a three-layer meander-line polarizer. Hence, before the performance evaluation of the final design, the structure description of the LP FRA, especially the phase distribution of every unit-cell in the main reflecting face and the antenna assembling detail, will be introduced clearly.

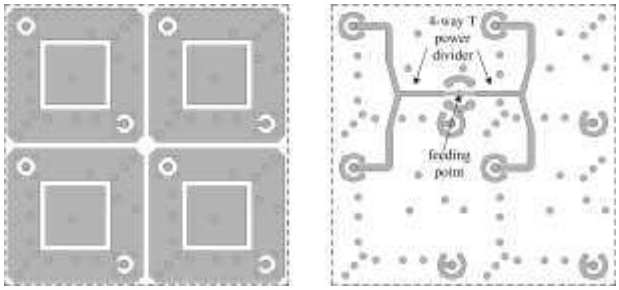

Fig.9. Layer 1 of the Central feeding array and the mating four-way power divider on Layer 4

The main reflecting face, which occupies about a 420×420 mm^2 ($L\times L\approx 49\lambda^2$) square area, is formed by 196 unit-cells, including 4 feeding elements in the central position, 52 unit-cells on the edge of the antenna aperture as protectors and rest for polarization twisting and phase compensating. The side length of every unit-cell is 28.5mm (~0.5λ). The

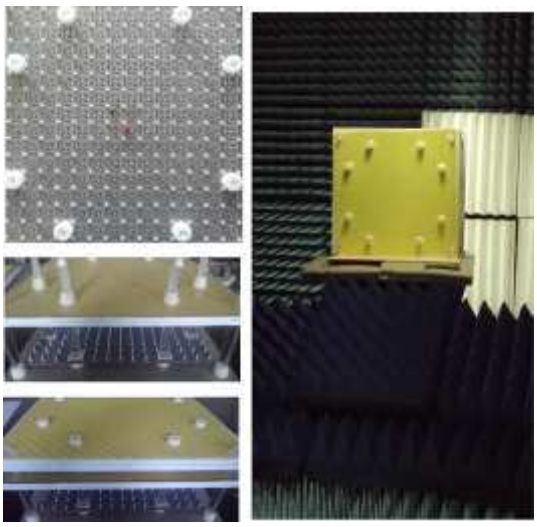

Fig. 13. Prototype of the presented LP and CP FRA

dimension of the polarizer grid, the meander-line polarizer and the square metal mounting plate is 500×500 mm^2.

As the two remarkable characteristics, the low profile and less volume are always preferred in the FRA. At the same time, the antenna efficiency should also be considered carefully. Thus, the focus-length-to-dimension (f/D) ratio becomes the key point in the whole antenna design.

In order to obtain the higher antenna gain based on the existing reflecting aperture and feeding array radiation pattern, the value of f/D=0.57 (the distance between the polarizer grid and main reflecting face is 120mm), which is a little larger than the typical value (f/D=0.5), is chosen for the presented FRA as a trade-off between antenna volume and aperture efficiency. According to this f/D value, the phase distribution on the reflecting face aperture could be figure out and then the phase delay-line length of every unit-cell at the corresponding position is selected from Fig. 5. With the purpose of obtaining a flat gain within the operating bandwidth, the phase compensation is accomplished at 5.1GHz.

The covering layer (Substrate 1) is mounted with nylon screws and nuts (M3). The polarization selecting grid is printed on FR4 board (with the thickness of 0.6mm) and supported by the low foamed polyvinyl chloride ($\varepsilon_{r1}\approx1.4$, $\tan\delta<0.002$) slab (with the thickness of 18mm). And then, the polarization selecting grid, the meander-line polarizer and the main reflecting face are mounted on the bottom metal plane through 12 plexiglass cylinder posts (Φ20 solid bar stock with M16 screw thread at two ends) with screwing nuts and washers. The antenna prototype is shown in Fig. 13.

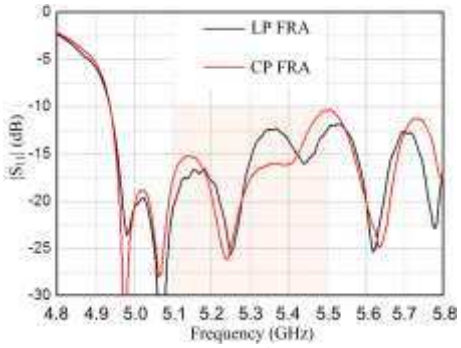

Fig.14. Measured $|S_{11}|$ result of the LP and CP FRAs

C. Measured results of the LP and CP FRAs

The testing procedure is as follows. Firstly, the LP FRA is assembled and the $|S_{11}|$ result is measured. Secondly, the meander-line polarizer is added and the $|S_{11}|$ result of the CP FRA is tested. The distance between the main reflecting face and the polarizer grid is slightly modified according to the obtained $|S_{11}|$ results. After that, the polarizer is removed and the radiation pattern and antenna gain test of the LP FRA as the important foundation is implemented and the measured results are obtained as the comparison with the later CP FRA results. Then, the meander-line polarizer is installed again and the radiation pattern, axial ratio and antenna gain of the CP FRA is obtained finally.

The measured $|S_{11}|$ of the LP and CP FRAs is shown in Fig. 14. Compared with the feeding array results, the bandwidth of both the LP and CP FRAs is quite wider than expectation. And the extra resonant valleys of the $|S_{11}|$ curve are caused by the multi-reflection in the broadside direction between the feeding array and the polarizer grid. The observed bandwidth is overrode the operating frequency range of the DP unit-cells. However, the extra bandwidth will not be possessed by the DP unit-cells with the inexistence of the multi-reflection situation. Thus, this fake bandwidth bonus will be ignored here. In addition, after assembling the meander-line polarizer, the $|S_{11}|$ curve gets a little higher at 5.5 GHz, but it is still lower than -10 dB.

The measured normalized radiation patterns of the LP FRA in both E- and H-planes at 5.1 GHz, 5.3 GHz and 5.5 GHz including the co-polarization and cross-polarization are displayed in Fig. 15. The 3 dB beamwidth is 8° at 5.1 GHz, and it increases to 9° at 5.5GHz. The maximum sidelobe level (SSL) is lower than -15 dB and -20 dB in E- and H-planes respectively. In addition, a high second SSL nearby -30° direction is observed, especially in E-plane pattern at 5.1GHz. The cross-polarization of the feeding array, whereas it becomes the co-polarization of the LP FRA, mainly contributes to this. Regarding the cross-polarization, benefit by the naturally polarization selecting function of the polarizer grid, the cross-polarization of the LP FRA could easily reach the -30 dB level within the 3 dB beamwidth range of the main lobe.

Fig. 16 shows that the measured antenna gain of the LP FRA is higher 21 dBi. Owing to the moderate defocusing at the high frequencies, the flat gain curve is obtained and the gain variation is less than 1 dB in the operating bandwidth.

After the evaluation of the LP FRA performance as the fundamental preparation, the meander-line polarizer is added on the top of the polarizer grid. In order to obtain the optimized performance, several assembling modifications have been done. The distance between the polarizer grid and the meander-line polarizer has been adjusted to 30mm, which is about a half wavelength (~0.5λ) for the operating frequencies. And also, the assembling angle of the meander-line polarizer has been swung anticlockwise, which is 43° along the grid vein. Then the working performance of the final CP FRA is characterized through the measured results.

The measured normalized radiation pattern and axial ratio of the CP FRA concentrating on the main-lobe angle range in two orthogonal main planes (the azimuth angle of φ=0° and φ=90°) are displayed in Fig. 17. After covering the polarizer the 3 dB beamwidth changes to 10° over the whole operating bandwidth, which is wider than the LP FRA. From the observation of the AR results, slight difference between two main planes at broadside direction has been observed. This phenomenon is caused by the beam misalignment between the standard horn antenna and the under-test CP FRA. Within the 3 dB beamwidth, the maximum axial ratio value of 2.5 dB is emerged in broadside direction at 5.1GHz. And the minimum axial ratio value falls down to 1dB in broadside direction at 5.3GHz.

Fig. 18 shows the measured antenna gain and axial ratio of the CP FRA over the operating bandwidth. The gain curve of the CP FRA is nearly as the same as the LP FRA, except the 0.4 dB gain loss in maximum caused by the material attenuation of the meander-line polarizer. In addition, the AR is lower than 2.5 dB all over the operating bandwidth. And in the high frequency range, the AR value is lower than 2 dB. Compared with simulation results of the unit meander-line in previous section, the AR performance deterioration is contributed by two main sources: one is that the sharp taper illumination of the main lobe produces the imperfect operating condition, which is different from the ideal periodicity in the simulation. The other one is the undesirable effect caused by the short distance between the polarizer grids and the meander-line polarizer. But even so, the measured AR results are still below 3 dB and satisfy the design requirement.

V. CONCLUSION

The design of a right-hand circular-polarized folded reflectarray antenna over the operating frequency range from 5.1 GHz to 5.5 GHz is presented in this paper. The circular polarization is achieved on the base of a traditional linear-polarized folded though combining with a meander-line polarizer. The design procedure is introduced in detail. And the antenna prototype has been fabricated and tested. The maximum 22 dB antenna gain is obtained and the measured axial ratio is below 2.5 dB over the operating bandwidth. The experimental results successfully demonstrate that the proposed design provides a feasible approach for the realization of the circular-polarized folded reflectarray.

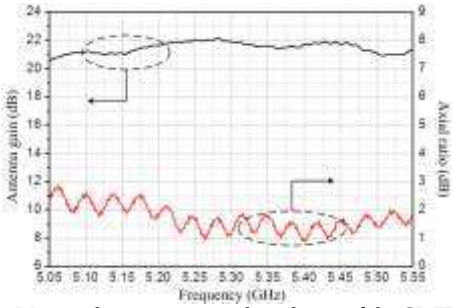

Fig. 18. Measured antenna gain and axial ratio of the CP FRA at the broadside direction

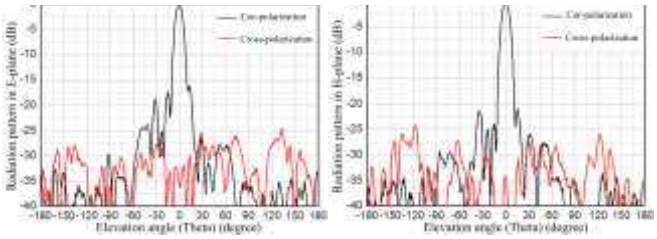

(b) 5.3 GHz

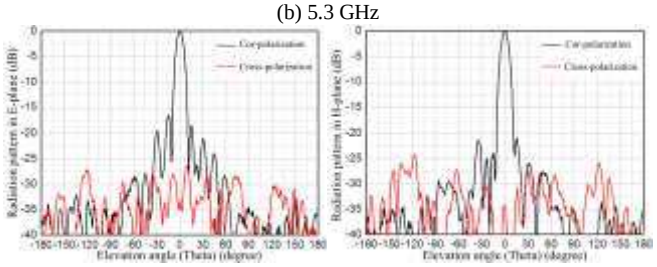

(c) 5.5 GHz

Fig.15. Measured normalized radiation pattern of the LP FRA in E-plane and H-plane at (a) 5.1 GHz (b) 5.3 GHz and (c) 5.5 GHz

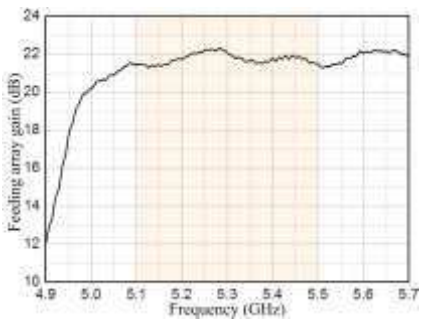

Fig. 16. Measured antenna gain of the LP FRA

ACKNOWLEDGMENT

The authors wish to acknowledge the funding of this work from 2013 Shaanxi Provincial Science and Technology Program sponsored by the Science and Technology Department of Shaanxi province, P. R. China under the research contract 2013KW02. Thanks to Mr. Yanping Ma at School of Electronics and Information, Northwestern Polytechnical University for assisting the antenna radiation pattern and axial ratio measurement.

REFERENCES

[1] J. Huang and J. A. Encinar, reflectarray antennas. Piscataway, NJ, USA: IEEE Press, 2008.

[2] D. Pilz and W. Menzel, "Folded reflectarray antenna," IET Electron. Lett., vol. 34, no. 9, Apr. 1998.

[3] A. Zeitler, J. Lanteri, C. Pichot, C. Migliaccio, P. Feil, and W. Menzel, "Folded reflectarray with shaped beam pattern for foreign object debris detection on runways," IEEE Trans. Antennas and Propag., vol. 58, no.9, pp.3065-3068, Sep, 2010.

[4] J. A. Zornoza, Ralf Leberer, J. A. Encinar, and W. Menzel, "Folded multilayer microstrip reflectarray with shaped beam pattern," IEEE Trans. Antennas and Propag., vol. 54, no.4, pp.510-518, Feb, 2006.

[5] M. Jiang, W. Hong, Y. Zhang, S. H. Yu and H. Zhou, "A Folded Reflectarray Antenna With a Planar SIW Slot Array Antenna as the Primary Source," IEEE Trans. Antennas and Propag., vol. 62, no.7, pp.3575-3583, July, 2014.

[6] J. J. Ren and W.Menzel,"Dual-Frequency Folded Reflectarray Antenna," IEEE Antennas Woreless Propagat. Lett., vol. 12, pp.1216-1219, 2013.

W. Menzel, D. Pilz and M. Al-Tikriti, "Millimeter-wave folded reflectarray antennas with high gain, low loss, and low profile," IEEE Antennas Propga. Mag., vol. 44, no. 3, pp. 24-29, June, 2002.Q. Luo, S. Gao, C. Zhang, D. Zhou, T. Chaloun, W. Menzel and V. Ziegler, "Design and Analysis of a Reflectarray Using Slot Antenna Elements for Ka band Satcom," IEEE Trans. Antennas and Propagation, Vol. 62, No. 4, April 2015, pp. 1365-1374

[7] T. Chaloun, W. Menzel, F. Tabarabi, T. Purtova, H. Schumacher, M. Kaynak, Q. Luo, S. Gao, R. Starec and V. Zieler "Wide-angle scanning active transmit/receive reflectarray," IET Microwaves, Antennas &Propagation, vol. 8, iss. 11, pp. 811-818, Aug. 2014.

[8] S. Gao, Q. Luo and F. Zhu, Circularly Polarized Antennas, Wiley (UK)-IEEE Press (USA), Jan. 2014

[9] L. Young, L. A. Robinson and C. hacking, "Meander-line polarizer," IEEE Trans. Antennas and Propag., vol. 21, no.3, pp.376-378, May, 1973.

[10] B. A. Munk, Finite antenna arrays and FSS. New York: John Wiley & Sons, 2003.

[11] M. A. Joyal and J. J. Laurin, "Analysis and design of thin circular polarizers based on meander lines," IEEE Trans. Antennas and Propag., vol. 60, no.6, pp.3007-3011, June, 2012.

[12] C. Zhang, G. Wei, J. Z. Li, F. Qin and S. Gao, "Dual-polarized unit-cell element for wide-angle electrically beam- scanning reflectarray," 2014 Loughborough antennas and propagation conference (LAPC), pp. 457-460, Nov. 2014.

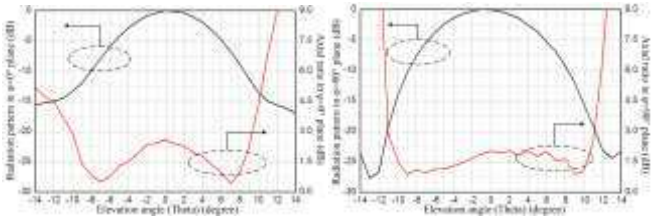

(a) 5.1 GHz

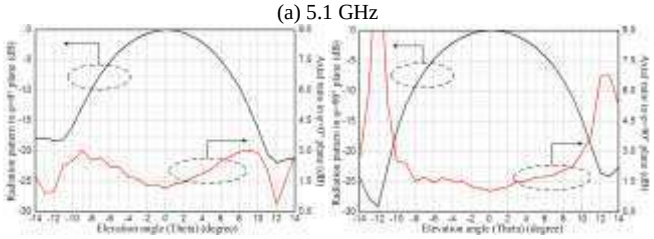

(b) 5.3 GHz

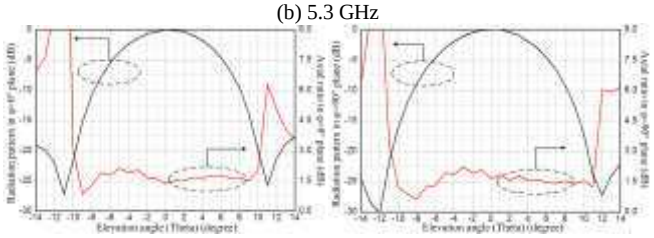

(c) 5.5 GHz

Fig.17. Measured normalized radiation pattern and axial ratio of the CP FRA in two orthogonal main planes (φ=0° and φ=90°) at (a) 5.1 GHz (b) 5.3 GHz and (c) 5.5 GHz